A METHOD FOR DERIVING LAND SURFACE MOISTURE, VEGETATION OPTICAL DEPTH, AND OPEN WATER FRACTION FROM AMSR-E

Lucas A. Jones[1,2], John S. Kimball[1,2], Erika Podest[3], Kyle C. McDonald[3], Steven K. Chan[3], Eni G. Njoku[3]

[1]Numerical Terradynamic Simulation Group, University of Montana, Missoula, MT
[2]Flathead Lake Biological Station, University of Montana, Polson, MT
[3]Jet Propulsion Laboratory, California Institute of Technology, Pasadena, CA

ABSTRACT

We developed an algorithm to estimate surface soil moisture, vegetation optical depth and fractional open water cover using satellite microwave radiometry. Soil moisture results compare favorably with a simple antecedent site precipitation index, and respond rapidly to precipitation events indicated by TRMM. High optical depth reduces soil moisture sensitivity in forests and croplands during peak biomass, although tundra locations maintain soil moisture sensitivity despite high optical depth. Optical depth varies with characteristic seasonality across vegetation cover types and tracks measures of vegetation canopy cover from MODIS. The algorithm developed in this study is able to monitor the daily variability of several important land surface state variables.

Index Terms— AMSR-E, microwave radiometry, soil moisture, vegetation, water resources.

1. INTRODUCTION

Vegetation canopy biomass, surface coverage of open water and surface soil moisture strongly influence land-atmosphere fluxes of water vapor, energy and trace gases. These factors have potentially large and uncertain feedbacks with climatic change. High-latitude, monsoonal, and semi-arid regions are particularly affected. Satellite optical-IR remote sensing, such as the Normalized Difference Vegetation Index (NDVI) and Leaf-Area Index (LAI), is commonly used to determine vegetation canopy cover. However, clouds, aerosols, and solar illumination effects limit the temporal repeat, spatial coverage and accuracy of these observations.

Several methods are available for determining surface soil moisture using microwave radiometry. These methods typically account for vegetation attenuation of the microwave signal using optical-IR remote sensing derived NDVI, or simultaneously solve for soil moisture and vegetation optical depth using multi-frequency brightness temperatures [1, 2]. Fractional coverage of open water bodies (*fw*) within the satellite footprint can contaminate retrievals of soil moisture and vegetation optical depth because the high dielectric of even relatively small water bodies reduces the bulk emissivity of the footprint much more than an equivalent coverage of soil at field capacity. Current approaches ignore *fw* bias, adjust for it using static land cover maps, or mask suspected areas.

While inland open water bodies may not represent a significant portion of the global land area, *fw* can represent a significant portion of landscapes where remotely-sensed soil moisture and vegetation information is desirable, including boreal forest, tundra, and agricultural lands. Open water in these areas is by no means static and flooding of riparian areas, irrigated fields and recharge and drying of wetlands occur seasonally. The *fw* term is therefore an important geophysical variable worthy of satellite monitoring.

We developed a method for global mapping and monitoring of vegetation optical depth, surface soil moisture and *fw* using satellite multi-frequency microwave remote sensing from the Advanced Microwave Scanning Radiometer on EOS (AMSR-E). We applied these methods to assess spatial patterns and temporal variability in these parameters over the northern hemisphere. We use *in situ* measurements and complementary satellite observations to determine the relative accuracy of our estimates.

2. APPROACH

We use the AMSR-E 18.7 GHz H and V polarized brightness temperatures (*Tb*) to estimate vegetation optical depth and open water fraction and use the 10.7 GHz H polarized *Tb* to estimate soil moisture. We use the descending (AM) overpass, but methods can be extended to the ascending (PM) overpass time. Methods can also be extended to 6.9 GHz *Tb* where it is not susceptible to radio-frequency interference. Data are gridded to the 25-km

Equal Area Scalable Earth (EASE) Grid from the Level 2A data product using inverse distance squared weighting [3].

Physical near-surface air temperature (*Ts*), *fw*, and vertically integrated atmospheric water vapor (*V*) are estimated using AMSR-E 18.7 and 23.8 GHz, H and V polarized *Tb* according to [4]. We then use *Ts* and *V* to calculate the effective emissivity of polarization *p* for each channel,

$$ep = \frac{Tbp/Ts - (1 - t_a(V))\Delta T}{t_a(V)}$$

where the atmospheric transmissivity (t_a) is a function of *V* and oxygen absorption, and the ΔT weights integrated atmospheric and surface temperatures.

We apply these results to calculate a slope parameter (*a*),

$$a = \frac{ev - ev_{wat}}{eh - eh_{wat}}$$

open water emissivities (ev_{wat}, eh_{wat}) are considered constant, although they are potentially increased by water waves, foam, and salinity. The slope parameter gives a quantity sensitive to vegetation and surface roughness, which is orthogonal to *fw* variability. The slope and daily *fw* quantities are temporally smoothed using a moving window median time domain filter. Open water decreases the bulk pixel sensitivity of *Tb* to soil moisture much more slowly than a proportional amount of vegetation optical depth (Fig. 1).

The effective optical depth of the land fraction (τ_c) is determined by inverting the so-called τ-ω equation in terms of the slope (*a*),

$$A = (1 - \omega)(rv_s - a * rh_s)$$

$$B = a * eh_s - ev_s + (1 - \omega)(a * rh_s - rv_s + 1 - a)$$

$$C = (1 - \omega)(a - 1) + ev_{wat} - a * eh_{wat}$$

$$\tau_c = \frac{-B - \sqrt{B^2 - 4AC}}{2A}$$

where the bare, dry soil emissivities (eh_s, ev_s) and vegetation single scattering albedo (ω) determine potential maximum and minimum slopes, respectively, and rh_s and rv_s are found by Kirchhoff's Law. The 18.7 GHz channel derived τ_c is then proportionality adjusted to estimate τ_c for the 10.7 GHz channel [5].

Surface soil moisture (<2 cm depth) is derived using the effective emissivity of the AMSR-E 10.7 GHz, H polarized *Tb* by inverting the τ-ω equation and a simple polynomial approximation of the Dobson dielectric model and Fresnel equations for loam soils. The variance in estimated soil reflectivity, and hence surface soil moisture, is inversely proportional to 1-*fw*. We therefore dampen the variability by the factor 1-*fw*, which improves the dynamic range of estimates under marginal conditions.

3. VALIDATION

3.1. Methods

We assessed relative accuracy of the retrievals using *in situ* measurements and independent satellite observations of complementary variables. We selected 2003 daily meteorological information from a latitudinal transect of five flux tower sites within regionally dominant land cover types. We calculated a simple antecedent moisture index from *in situ* daily precipitation measurements for comparison with the AMSR-E soil moisture retrievals, as soil moisture measurements are frequently unreliable and taken from depths that are too deep for accurate comparison with microwave remote sensing [6]. We then normalized the *in situ* moisture index and AMSR-E derived soil moisture values to assess relative agreement of variability.

We use 0.25° gridded satellite daily cumulative rainfall from Tropical Rainfall Monitoring Mission (TRMM) merged with Global Precipitation Index (GPI) calibrated monthly IR products to assess relative agreement between regional precipitation events and AMSR-E derived soil moisture patterns and temporal cycles of wetting and drying [7].

We compared AMSR-E derived *fw* results with similar *fw* maps derived from Japanese Earth Resource Satellite (JERS-1) 100-m and Moderate Resolution Imaging Spectro-radiometer (MODIS) 1-km resolution land cover classifications [8]. The *fw* is calculated as the sub-grid scale fractional coverage of open water when the two land cover datasets are binned to the 25-km EASE grid. Timeseries were extracted from two sites located on the Yukon River to assess *fw* seasonality.

3.2. Site Comparison

The AMSR-E soil moisture retrievals respond rapidly to precipitation wetting and dry quickly (within 2-5 days) in the absence of additional rainfall (Fig. 2). AMSR-E soil moisture corresponds closely to the *in situ* precipitation index measurements when $\tau_c < 1.2$. Soil moisture accuracy is reduced for boreal forest and for the cropland location during peak LAI, as indicated by insignificant correlations. However, the cropland site apparently responds to precipitation events prior to peak LAI. Interestingly, the tundra location has a higher peak τ_c than either the boreal forest or the cropland, yet maintains more sensitivity to soil moisture; this may be the result of saturated, radiometrically absorptive organic matter underlying a highly porous organic surface layer characteristic of tundra.

The AMSR-E τ_c seasonality agrees well with the timing of peak MODIS LAI at all locations. The boreal forest τ_c also varies seasonally, which is likely due to deciduous vegetation in disturbed locations or within mixed evergreen and deciduous forest canopies. The cropland location is dominated by corn and soybeans, where τ_c peaks as crops mature in August. The τ_c over desert grasslands shows two seasonal peaks corresponding to characteristic vegetation growth during monsoonal rainfall periods evident in the AMSR-E soil moisture time series.

3.3. Regional Map Comparison

The AMSR-E derived daily soil moisture series is responsive to periodic wetting events indicated by TRMM (Fig. 3). These results concur that the AMSR-E soil moisture retrievals reflect a relatively shallow soil layer with characteristic rapid wetting and drying cycles in response to precipitation events. Widespread precipitation indicated by TRMM occurs in the upper Midwest on June 2 and June 5 and in the vicinity of Oklahoma and Kansas on June 3 and June 4, 2003. These events coincide with AMSR-E derived soil moisture increases the following day. Soil moisture wetting from a June 1 precipitation event is also evident in the Southwestern Sahel and this patch persists for the following three days. Another persistent patch of high soil moisture is evident over Turkey in response to a band of light precipitation that persists for three days. The AMSR-E soil moisture maps appear free from water contamination along coastlines, rivers and other water bodies indicating the *fw* estimate effectively mitigates bias.

Estimated spatial water coverage of the entire Alaska region is 4.8 %, 4.4 %, and 3.4 % for JERS-1, AMSR-E, and MODIS, respectively. The AMSR-E *fw* map is spatially smooth relative to the aggregated JERS-1 derived *fw* map (Fig. 4). This is mainly an artifact of spatially aggregating the relatively fine scale JERS-1 land cover and the smoothing inherent in re-sampling of the egg-shaped AMSR-E swath footprints to a 25-km earth grid. However, the AMSR-E product retains sub-grid scale information on inundated wetlands and small lakes that is missing from the 1-km MODIS classification, as indicated by a larger regional *fw* value.

The AMSR-E derived *fw* variable provides daily estimates of open water area over Alaska (Fig. 5). These results show large differences in spatial and seasonal *fw* patterns across the region, including two locations within the Yukon River basin. The Yukon Delta location is within a large wetland and is located further south and closer to the coast than Stevens Village, and therefore shows an earlier spring thaw, later fall freeze and larger *fw* area. The steep rise and fall in the seasonal *fw* signal occurs as lake and river ice melts in the spring and freezes in fall; this pattern coincides with the annual cycle of inundation and drying of abundant seasonal wetlands, especially over the Yukon Delta region.

4. CONCLUSION

We have developed an algorithm to estimate fractional open water coverage, vegetation optical depth and surface soil moisture using multi-frequency brightness temperatures from AMSR-E. The results of this study indicate that the soil retrievals are reasonably accurate under low optical depth conditions ($\tau_c < 1.2$), as well as for high optical depth in tundra. Soil moisture retrieval accuracy is reduced to non-existent over high optical depth forest and cropland locations during peak biomass. The AMSR-E optical depth retrievals show characteristic seasonality across a range of North American land cover types and agree well with alternative canopy cover estimates from MODIS LAI. Dynamic open water fraction retrievals effectively mitigate potential soil moisture bias and provide an additional important hydrological parameter for global monitoring. Open water is a key component of continental seasonality, especially for boreal forest, tundra, wetland, riparian, and irrigated ecosystems. The results of this study indicate that algorithms for upcoming satellite microwave soil moisture missions, such as SMAP and SMOS, should consider dynamic corrections for open water.

ACKNOWLEDGEMENTS

This study was conducted as the University of Montana and the Jet Propulsion Laboratory under contract to the National Aeronautics and Space Administration. The authors thank the site investigators for use of precipitation data.

REFERENCES

[1] Owe, M., R. de Jeu, and J. Walker, "A methodology for surface soil moisture and vegetation optical depth retrieval using the microwave polarization difference ratio," *IEEE Trans. Geosci. Rem. Sens.*, 39(8), pp. 1643-54, 2001.

[2] Jackson, T. J., et al., "Soil moisture mapping at regional scales using microwave radiometry: The Southern Great Plains Hydrology Experiment," *IEEE Trans. Geosci. Rem. Sens.*, 37(5), pp. 2136-50, 1999.

[3] Ashcroft, P., and F. Wentz, "Algorithm Theoretical Basis Document: AMSR level 2A algorithm," *RSS Tech. Report*, 121 599B-1, Santa Rosa, CA, 1999.

[4] Jones, L. A., et al., "Daily land surface air temperature retrieval from AMSR-E: Comparison with AIRS/AMSU," *IEEE J-STARS*, (in review).

[5] Njoku, E. G. and S. K. Chan, "Vegetation and surface roughness effects on AMSR-E land observations," *Rem. Sens. Environ.*, 100, pp. 190-99, 2006.

[6] Wagner, W., G. Lemione, and H. Rott, "A method for estimating soil moisture from ERS Scatterometer and soil data," *Rem. Sens. Environ.*, 70, pp. 191-207, 1999.

[7] Huffman, G.J., et al., "The Global Precipitation Climatology Project (GPCP) combined precipitation dataset," *Bul. Amer. Meteor. Soc.*, 78, pp. 5-20, 1997.

[8] Whitcomb, J., M. Moghaddam, K. McDonald, J. Kellndorfer, E. Podest. "Mapping vegetated wetlands of Alaska using L-band radar satellite imagery," *Can. J. Rem. Sens.*, 35(1), pp. 54-72, 2009.

FIGURES

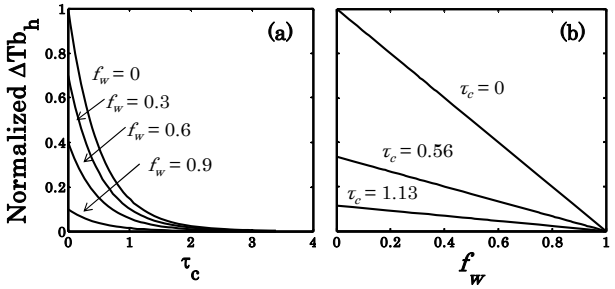

Figure 1: Normalized H polarized *Tb* range from dry (0.05 vol.) to wet (0.50 vol.) soil with changing optical depth (τ_c) and open water fraction (f_w).

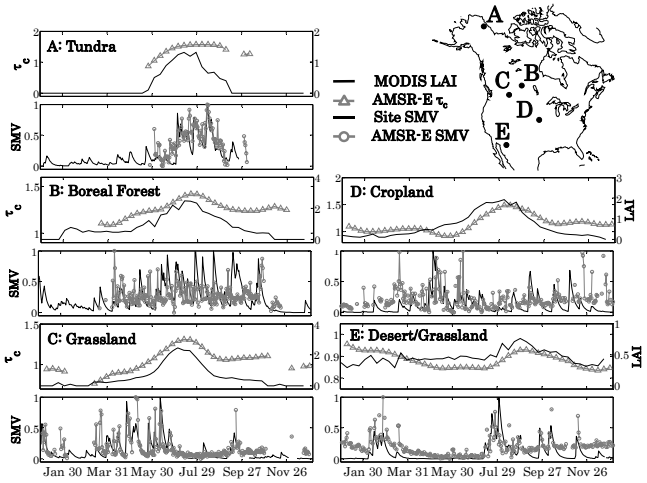

Figure 2: Comparison of AMSR-E retrievals with antecedent precipitation (SMV), and comparison of AMSR-E τ_c seasonality with MODIS LAI for five study locations. SMV is normalized to the unit interval to compare variability. The vegetation plot y-axes are scaled to show variability.

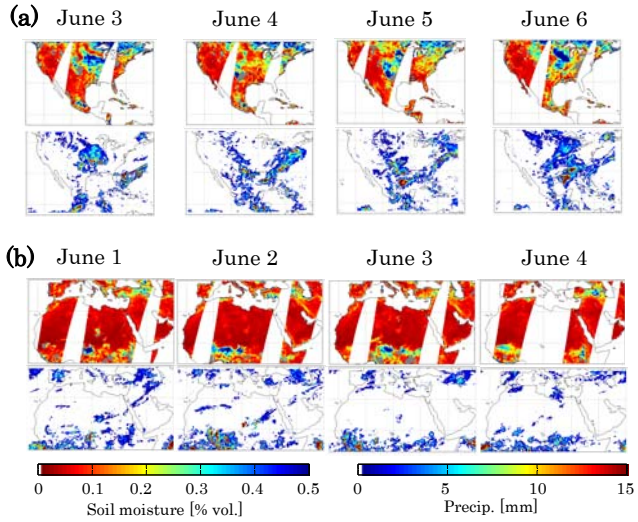

Figure 3: AMSR-E daily soil moisture retrievals for successive days and TRMM prior 24-hour cumulative precipitation for (a) the continental U. S. and (b) Northern Africa, Middle East, and Asia Minor.

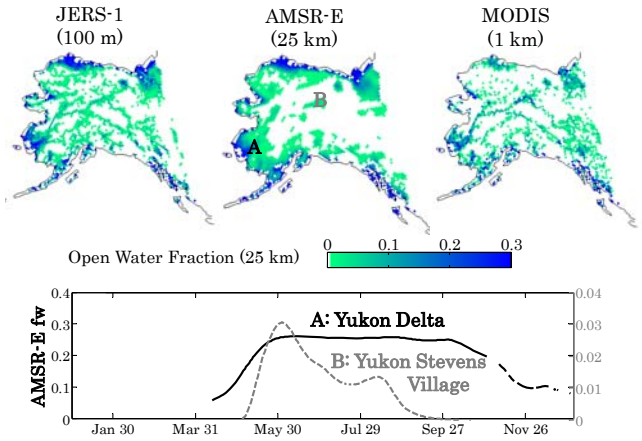

Figure 4: Comparison of gridded 25-km open water estimates for Alaska. The resolutions listed below the instrument names indicate the product native resolution prior to gridding. The JERS-1 product is from [8]. Open water seasonality retrieved by AMSR-E is shown for two locations for 2003.